Applied Surface Science 501 (2020) 144027

Contents lists available at ScienceDirect

Applied Surface Science

journal homepage: www.elsevier.com/locate/apsusc

Full Length Article

Zn-Al LDH growth on AA2024 and zinc and their intercalation with chloride: Comparison of crystal structure and kinetics

Anissa C. Bouali[a,*], Mariia H. Iuzviuk[b], Maria Serdechnova[a], Kiryl A. Yasakau[c], D.C. Florian Wieland[a], Gleb Dovzhenko[a], Hanna Maltanava[d], Igor A. Zobkalo[b], Mario G.S. Ferreira[c], Mikhail L. Zheludkevich[a,e]

[a] Institute of Materials Research, Helmholtz-Zentrum Geesthacht, Max-Planck-Straße 1, 21502 Geesthacht, Germany
[b] Petersburg Nuclear Physics Institute named by B.P. Konstantinov of National Research Centre «Kurchatov Institute», Orlova roshcha 1, 188300 Gatchina, Russia
[c] CICECO – Aveiro Institute of Materials, Dep. Materials and Ceramic Engineering, University of Aveiro, 3810-193 Aveiro, Portugal
[d] Research Institute for Physical Chemical Problems, Belarusian State University, 220030 Minsk, Belarus
[e] Faculty of Engineering, Kiel University, Kaiserstraße 2, Kiel 24143, Germany

ARTICLE INFO

Keywords:
Layered double hydroxide
Anion exchange
Crystal structure

ABSTRACT

The dissimilarities and features of the crystal structure of ZnAl LDH-NO_3 conversion layers grown directly on pure zinc and aluminum alloy 2024 were investigated in the present paper. Although the nature of the cations in the double hydroxides are the same in both cases (Al^{3+} and Zn^{2+}), their sources differ according to the substrate. This leads to a difference in the cationic layers and interlayer structure, which consequently influences the anionic exchange reaction. In the frame of this work, the kinetics of the anion-exchange of nitrate by chloride was investigated as well as the crystal structure of the resulting ZnAl LDH-Cl on both substrates. Synchrotron high-resolution X-ray diffraction was the main method to obtain structural information and was supported by additional calculations and scanning electron microscopy.

The current study revealed noticeable changes on the positioning of the interlayer atoms for the ZnAl-LDH-Cl on zinc in comparison with the ones on AA2024 substrate.

1. Introduction

The application of conversion coatings on metallic materials such as steel, aluminum alloys and magnesium alloys is a widely used method for corrosion protection [1–6]. It generally involves an electrochemical or chemical modification of the material surface leading to the formation of a layer, which creates a physical barrier and improves adhesion to the consecutively applied polymer coatings allowing a better resistance against corrosion attack. However, in many cases, the physical barrier alone is not sufficient since once the latter is perforated due to defects or scratches, corrosion is inevitable.

Therefore, recently many studies were focused on the development of self-healing corrosion protective systems, but with the main aim of replacing the detrimental Cr(VI)-based conversion coatings due to their toxicity and harmful impact on the environment [7–9]. The focus of these studies was oriented to the “smart” delivery systems with the capacity to store corrosion inhibiting agents and release them when triggered by changes of pH, presence of corrosive species or mechanical damage [10–14]. Among these “smart” systems, layered double hydroxides occupy an important position as potential delivery systems for promoting an active corrosion protection of different metal alloys [15–20].

Layered double hydroxide (LDH) is part of the class of anionic clays belonging to brucite-like structures. They can be represented by the formula $[M^{II}_{1-x}M^{III}_{x}(OH)_2]^{x+}(A^{y-})_{x/y}\cdot zH_2O$, where M and A^{y-} correspond to metallic and anionic species, respectively [21–23]. The isomorphous substitution of some of the M^{II} cations in the brucite-like layers by a trivalent M^{III} cation leads to the generation of a stacking of positively charged sheets. This positive charge is balanced by anions (separated by water molecules) intercalated in the galleries between these mixed (M^{II}-M^{III}) hydroxide layers. The flexibility in terms of metal ions variation (both M^{II}, M^{III}) as well as their ratio (x) and change of anions in the interlayer gives rise to a large class of isostructural materials, which are very attractive in a broad range of applications [22,24].

In the past decade, the use of LDH nanocontainers in the field of corrosion protection has considerably evolved due to the anion-exchange aptitude of LDH [19,25–28]. This ability of easy anion-exchange

* Corresponding author.
E-mail address: anissa.bouali@hzg.de (A.C. Bouali).

https://doi.org/10.1016/j.apsusc.2019.144027
Received 15 July 2019; Received in revised form 3 September 2019; Accepted 13 September 2019
Available online 01 October 2019

can be exploited as a mean for corrosion protection in two separate but complementary ways:

(1) host for corrosion inhibitors in anionic form between the interlayers and their release *on demand* when triggered by changes at the interface (e.g. pH change) or presence of corrosive species (e.g. Cl^-, SO_4^{2-}…) [16,29].
(2) uptake of corrosive species in the galleries, behaving as *nanotraps* [26], while inhibitor is released.

Following the pioneer works of Buchheit *et al.* [30,31], a lot of effort has been devoted to LDH growth as a conversion coating on active metals with the main focus on the corrosion protection of aluminium and magnesium alloys [16,19,20,26,32,33]. However, recently the method was extended to other metallic substrates such as zinc, aiming equally to the corrosion protection of zinc galvanized steel structures [17,31].

The cations (Zn^{2+}, Al^{3+}) involved in the *in-situ* Zn-Al LDH conversion layer formation on both aluminium and zinc substrates, are the same. The only difference resides on the source of these cations. In the case of the aluminium substrate, Al^{3+} will be generated from the dissolution of the aluminium substrate itself [16] whereas Zn^{2+} will be generated from the dissolution of the zinc substrate [34].

This could implicate an apparent difference on the final formed LDH structure and morphology.

In the present study, we investigated possible discrepancies in the formation of Zn-Al LDH-NO_3 on a pure zinc substrate and on an AA2024 aluminium alloy. Furthermore, chloride was chosen as a model anion to investigate the anion exchange reaction in these two systems since it works as a main trigger for release of inhibitors when LDH is used for corrosion protection.

2. Materials and methods

2.1. Materials

2.1.1. Reagents

The chemicals used in the current work are aluminum nitrate nanohydrate ($Al(NO_3)_3{\cdot}9H_2O$, > 99%, Sigma-Aldrich, Germany), zinc nitrate hexahydrate ($Zn(NO_3)_2{\cdot}6H_2O$, > 99%, CarlRoth, Germany), ammonium nitrate (NH_4NO_3, > 98.5%, Bernd Kraft, Germany), ammonia solution ($NH_3{\cdot}H_2O$, 25%, Merck KGaA, Germany), sodium nitrate ($NaNO_3$, > 99.95, Sigma-Aldrich, Germany), sodium chloride (NaCl, 96%, AlfaAesar, Germany) and deionized water Millipore™ > 18.3 MΩ.

2.1.2. Substrates

The test samples and their compositions are described below:

a) Aluminum substrate: AA2024 (see Table 1)

b) Zinc substrate: zinc (see Table 2)

The size of the substrates in both cases was 10 × 10 mm and the specimens were polished using a 2500 SiC paper, rinsed with deionized water and left to dry at room temperature under air conditions.

2.2. Methods

2.2.1. LDH growth on zinc

The synthesis procedure employed in this work was reported in a recent publication by Mikhailau *et al.* [34]. Briefly, Zn-Al LDH-nitrate was grown on zinc substrates in 1 mM solution of $Al(NO_3)_3$ and 0.1 M $NaNO_3$ at pH 3.2 and temperature 90 °C. The source for the Zn element is provided by a dissolution of the zinc substrate.

The synthesis time has been adjusted to achieve the best result in terms of LDH phase structural uniformity. Care has been taken to remove carbon dioxide from water solutions reducing its impact onto structural properties of the synthesized LDH.

2.2.2. LDH growth on AA2024-T3

The LDH synthesis was performed according to the procedure described in previous works [16,25]. Zn-Al LDH-nitrate was grown in a hydrothermal bath containing $Zn(NO_3)_2$ (0.1 M) and NH_4NO_3 (0.6 M) (pH adjusted to 6.5 using 1% ammonia) under 95 °C for 30 min. In this case, the source for the Al element is provided by a dissolution of the AA2024 substrate.

The obtained Zn-Al LDH-NO_3 treated AA2024 and zinc samples were then moved to the set-up predisposed for the *in-situ* monitoring and study of the anion exchange reaction with NaCl (Fig. 1). The anion exchange step was carried out in a solution of 0.1 M NaCl at room temperature for 30 min.

For the sake of interpretation, the LDH-NO_3 and LDH-Cl will be denominated Zn-LDH-NO_3 and Zn-LDH-Cl when grown on zinc, and Al-LDH-NO_3, Al-LDH-Cl when grown on the aluminum substrate (AA2024).

2.3. Characterization

2.3.1. SEM and EDS analysis

The studied specimens were examined both in top and cross-sectional views using a Tescan Vega3 SB scanning electron microscope (SEM, Brno, Czech Republic) equipped with an *eumeX* energy dispersive X-ray (EDS, Heidenrod, Germany) spectrometer for the elemental composition analysis of the specimens.

2.3.2. Synchrotron X-ray diffraction

The study of the growth of LDH films on aluminum and zinc substrates as well as ion-exchange processes of the surfaces were carried out at the P08 high-resolution diffraction beamline from the PETRA III synchrotron radiation source (DESY, Hamburg, Germany) with an X-ray energy of 25 KeV [35]. The experimental set-up (Fig. 1) comprised an in-situ flow cell with a transparent window allowing the grazing incidence X-ray diffraction measurements. The cell was also connected to a neMESYS pump (CETONI GmbH, Korbussen, Germany) composed of a set of syringes, controlling the electrolyte solutions flow in and out of the cell. The ion exchange conditions (flow rate/change of solution and temperature) were controlled remotely using a software provided by the neMESYS. Therefore, it was possible to keep a hold onto the ion-exchange reaction while simultaneously performing the diffraction experiment.

The diffraction patterns were collected before the start of the anion-exchange reaction and then continuously recorded at an interval of 0.54 s after the start of the anion exchange. A two-dimensional PERKIN Elmer detector with a pixel size of 200 µm was used. The sample to detector distance was set to 1.426 m. The radial integration was performed using GSAS II package. Then results were analyzed and treated using the FAULTS [36] and AMORPH [37] softwares. FAULTS was utilized to refine the diffraction patterns and the identification of the atom positions, while AMORPH was used for the quantification of the present amorphous phases.

It is worth mentioning that the results described in this paper are

Table 1
Nominal composition of AA2024 in wt.%.

Component	Al	Cu	Fe	Cr	Mg	Mn	Si	Ti	Zn	Others
Wt.%	90.7–94.7	3.8–4.9	0.5	0.1	1.2–1.8	0.3–0.9	0.5	0.15	0.25	0.15

Table 2
Impurity content of zinc in wt.%.

Component	Zn	Pb	Cu	Cd	Sn	Ag	Ca	Fe	Si
Wt.%	99.95	0.02	0.003	0.002	0.001	0.0002	< 0.0001	< 0.0001	< 0.0001

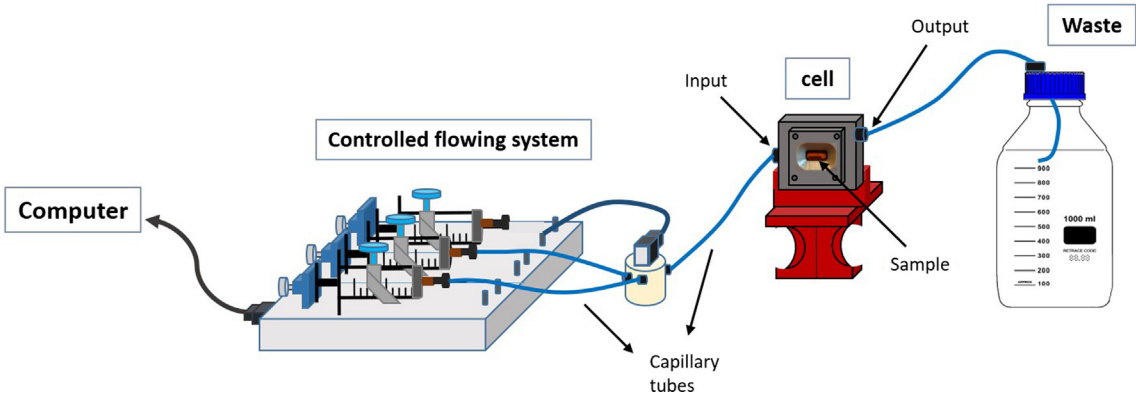

Fig. 1. Set-up used for controlling the solution flow and ion exchange reaction during synchrotron measurements.

specific to this experimental set up (Fig. 1) in terms of the cell geometry, flow rate, etc. The detailed study of influence of these particular parameters as well as features of anion exchange kinetics are not in the scope of the current study but will be investigated in future.

3. Result and discussion

3.1. SEM/ EDS results

Cross section SEM images of LDH-NO_3 prepared on zinc and AA2024 substrates are shown in Fig. 2.

The LDH conversion layer produced on zinc substrate has approximately 10–12 µm in thickness (Fig. 2.a) while the LDH on AA2024 is less than 1 µm (Fig. 2.b and c), apart from some zones where other effects (due to intermetallic) intervene to produce bigger flakes as demonstrated before [16].

The SEM planar view of the LDH layer grown on zinc and AA2024 are depicted in Fig. 3. Fig. 3.a and 3.b show zinc surface covered with LDH and with a typical plate-like structure. This perpendicular plate-like structure could not be witnessed with the cross-section image Fig. 2.a. The reason being that, the sample preparation may have been slightly aggressive and altered with the layered by crushing and damaging the structure.

At lower magnifications, some areas of the surface show a non-

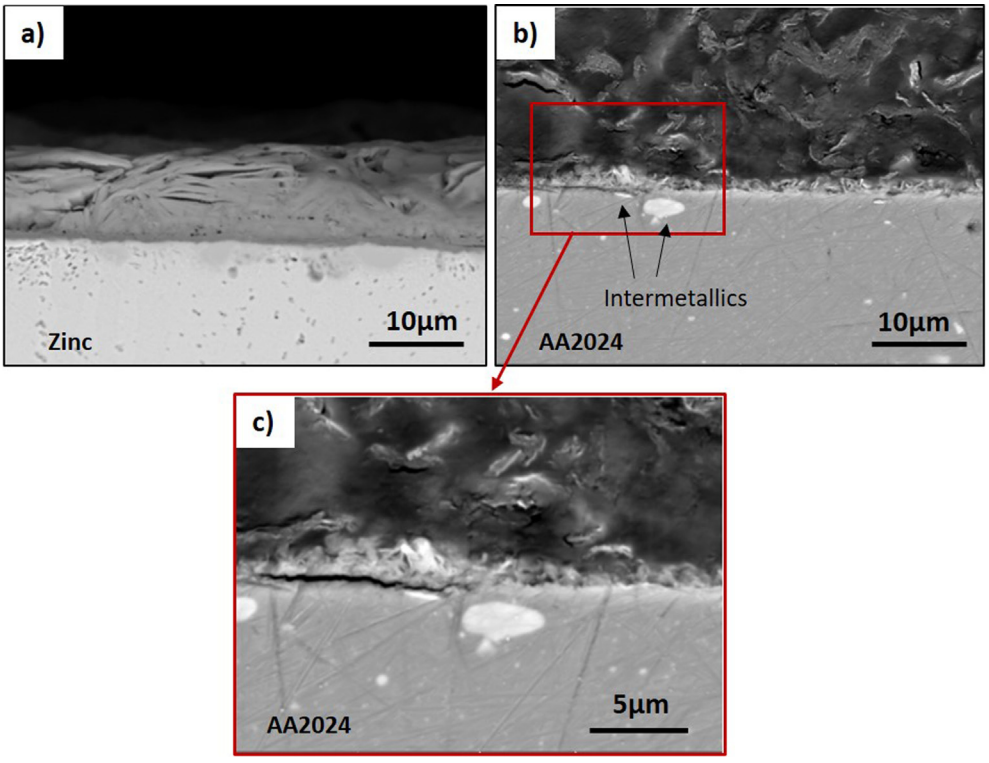

Fig. 2. SEM cross-section images of LDH-NO_3 grown on zinc substrate (a) on AA2024 substrate (b) and (c).

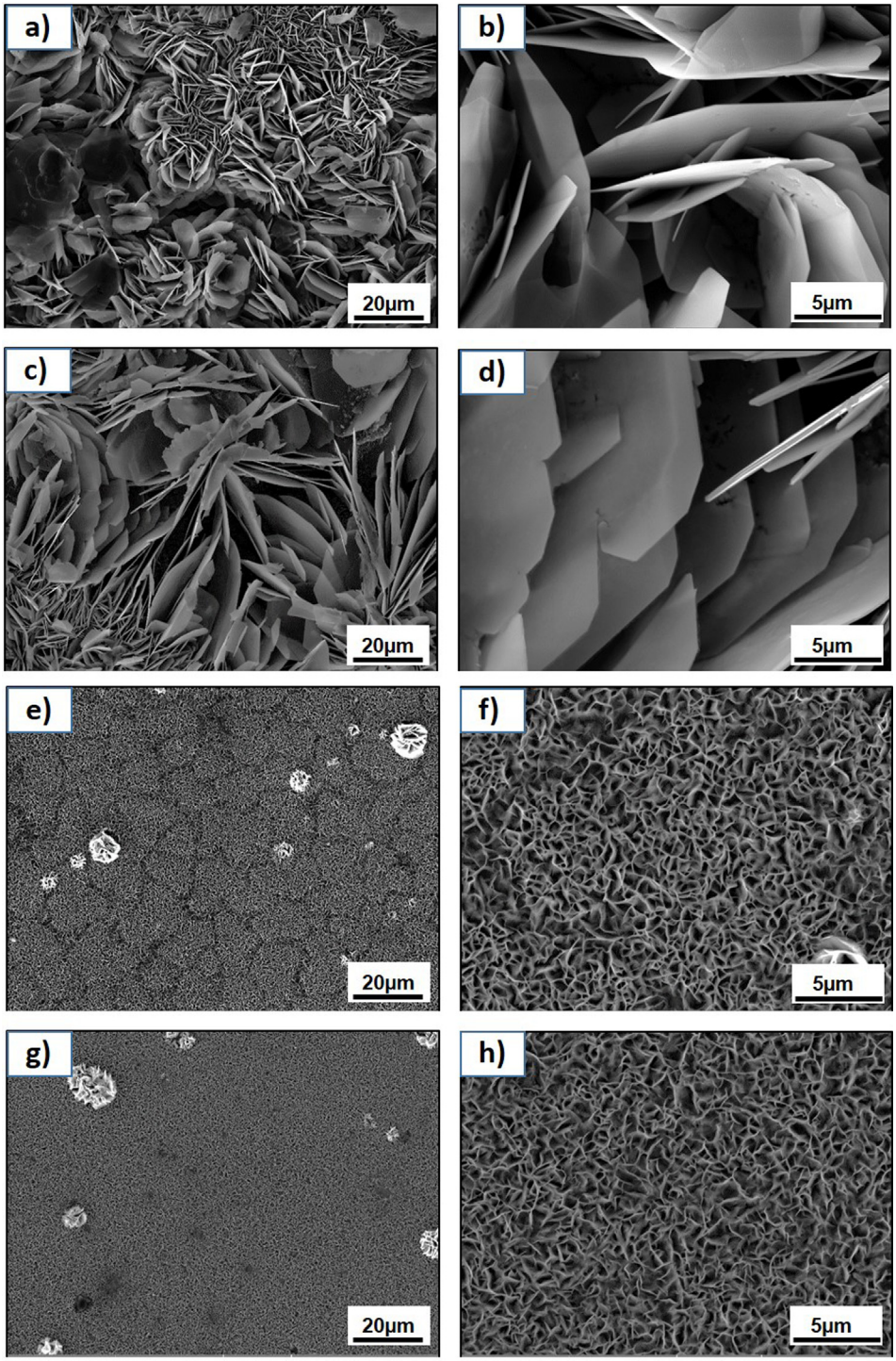

Fig. 3. SEM images of Zn-LDH-NO_3 (a) and (b), Zn-LDH-Cl (c) and (d), Al-LDH-NO_3 (e) and (f) and Al-LDH-Cl (g) and (h).

homogeneous distribution with respect to the size of the flakes. After an anion exchange reaction (duration 30 min) in a solution of 0.1 M NaCl, no visible changes in the surface morphology can be observed (Fig. 3.c and 3.d).

By comparing the LDH layers that were formed on the zinc substrate to the LDH formed on AA2024 substrate (Fig. 3.e and 3.f respectively), a different surface morphology can be seen. This morphology differs in terms of the flakes shape and size. Whereas the Zn-LDH-NO_3 and Zn-LDH-Cl flakes form an assembly of bigger and well-defined lamellas, the Al-LDH-NO_3 and Al-LDH-Cl present significantly smaller flakes aside from the zones of Cu-rich intermetallic, where large LDH islands can be observed due to the micro-galvanically induced dissolution of aluminum [38–41]. Similarly, to LDH on zinc, the overall LDH structure is preserved after the anion-exchange with Cl^- (Fig. 3.g and 3.h)

The EDS analysis of the surface is presented in form of two-dimensional maps (Fig. 4) followed by the extracted representative EDS spectra Fig. 5.

The EDS maps show an uneven distribution (Fig. 4) of the elements Al, Zn, N and O on both Zn-LDH-NO_3 and Zn-LDH-Cl (Fig. 4.a and b). Chloride is found only on Zn-LDH-Cl after the ion exchange reaction (Fig. 4. b). Although the LDH layer thickness on the zinc substrate is relatively homogeneous, the presence of Cl is noted only on some

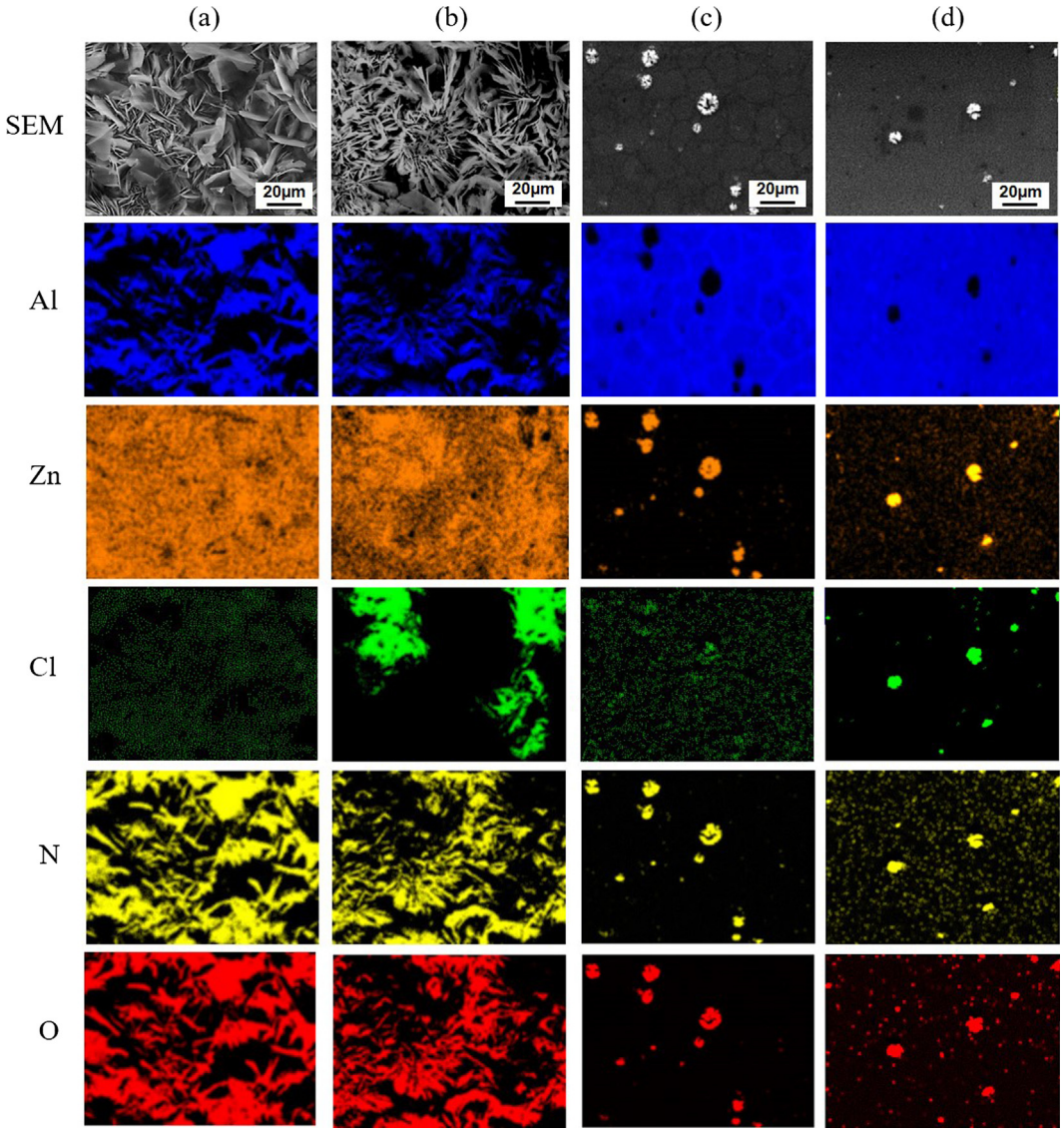

Fig. 4. EDS maps of Zn-LDH-NO_3 (a), Zn-LDH-Cl (b), Al-LDH-NO_3 (c), and Al-LDH-Cl (d).

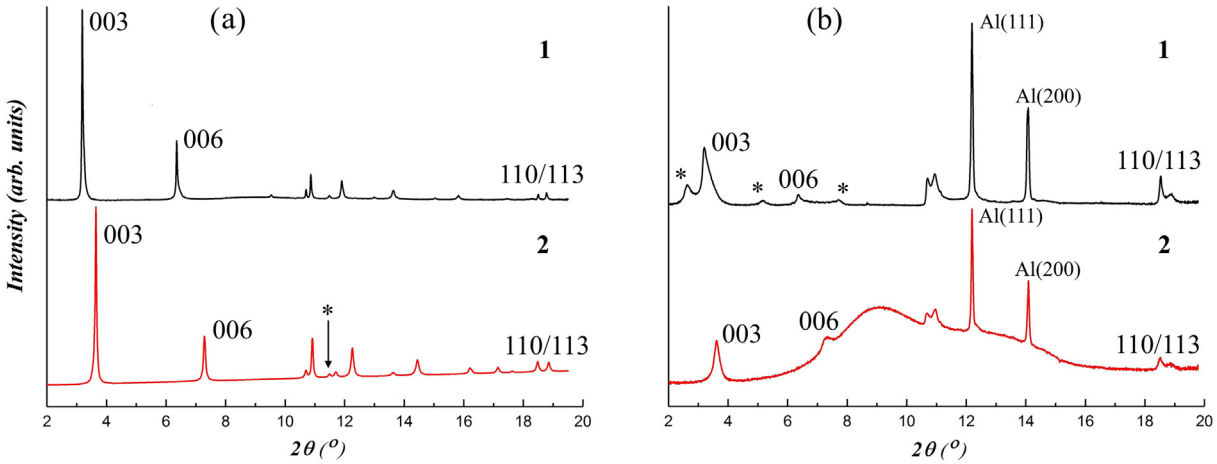

Fig. 5. (a) XRD patters of: 1 – Zn-LDH-NO_3 and 2 – Zn-LDH-Cl with subtracted amorphous contribution; (b) XRD patterns of: 1 – Al-LDH-NO_3 and 2 – Al-LDH-Cl (2). Non-LDH peaks are labeled by *.

specific zones. These specific zones are also enriched in zinc, this might entail that the anion-exchange between NO_3^- and Cl^- has led as well to the formation of intermediate phases with a complex Zn and Cl composition. This can be verified later in the text by the XRD analysis.

In the case of LDH film on Al alloy substrate, the same elemental distribution can be observed (Fig. 4.c and d). But contrary to LDH on Zn substrate, here, the elements are mainly accumulated at the thicker LDH islands. Due to the difference in the thickness of the LDH layers for the different substrates (Zn-LDH-NO_3 and Zn-LDH-Cl are thicker than Al-LDH-NO_3 and Al-LDH-Cl, respectively) and on the AA2024 alloy itself (between the LDH islands and the rest of surface), less X-ray emission (at Zn and Cl energies) comes from thinner areas in comparison the thicker zones. The difference in the total accumulation of the signals leads to the observation of a clear contrast on the elemental distribution maps.

Moreover, it can be seen that after anion-exchange with chlorides (Fig. 4.d), the Cl element is present on the same sites where Zn is found. This is an indication of the successful intercalation of Cl^- between the LDH interlayers.

3.2. X-ray diffraction analysis

The XRD pattern of the LDH-NO_3 on the zinc substrate demonstrates a single-phase LDH with a good crystallinity (Fig. 5.a). The crystal structure was successfully refined with FAULTS software [36], within the rhombohedral space group R-3m. For the refinement three-layered polytypes $3R_1$ (2/3, 1/3, 1/3) and $3R_2$ (1/3, 2/3, 1/3) were taken, which denote the trigonal prismatic and octahedral arrangements of hydroxyl groups in adjacent layers, respectively (Fig. 6) [22]. Moreover, additional non-LDH peaks (marked by an asterisk in Fig. 5) could be identified. These peaks could not be properly assigned, but this brings us back to the EDS results described above. In the case of the pattern in Fig. 5.a-2, the peak indicated by an asterisk and arrow may be assigned to the formation of zinc hydroxide chlorides as intermediates. The latter share some similar features with LDH [42].

It is worth emphasizing that for the refinement process, the water background was subtracted for all patters excluding the pattern in Fig. 5.b-2. The latter representing the Al-LDH-Cl, could not be refined after subtraction of water background. Whereas for the other spectra, the background subtraction did not alter with the crystal structure refinement.

The obtained values of the crystal structure parameters are given in Table 3. The cell parameter *c* for Zn-LDH-NO_3 equals to 26.862(9) Å and is close to that one reported in previous works [43,44]. This *c* value allows to conclude that in Zn-LDH-NO_3, nitrate ion plane makes a sufficiently large angle with the metal hydroxide layer - close to ~70° as it was established in [43] and is represented in Fig. 7. This situation clearly corresponds to a high cation layer charge and a Zn:Al ratio to be equal to 2:1 [43,45]. Indeed, refinement of the structures were made with other Zn:Al ratios but only a the ratio 2:1 provided a consistent agreement between the experimental and calculated XRD patterns. Moreover, in a work by S. Marappa *et al.* [43], several compositions with different Zn:Al ratios were studied. At a high layer charge ($x \sim 0.33$, i.e. Zn:Al = 2:1), the authors obtained an angle equal to ~70° between NO_3^- and hydroxide layers. This makes sense since for compensation of the high charged cation layers, it is necessary to pack plain NO_3^- anions as close as possible. Therefore they tend to be perpendicular to these cation layers.

Table 3
Unit cell parameters, basal spacing and gallery heights of Zn-LDH and Al-LDH.

Composition	a, Å	c, Å	d, Å	h, Å
Zn-LDH-NO_3	3.0771(2)	26.862(9)	8.954(3)	4.244(3)
Al-LDH-NO_3	3.0671(3)	26.70(1)	8.900(3)	4.190(3)
Zn-LDH-Cl	3.081(2)	23.359(5)	7.786(2)	3.076(2)
Al-LDH-Cl	3.076(1)	23.38(2)	7.793(7)	3.080(7)

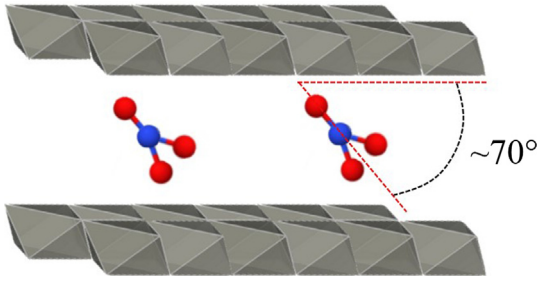

Fig. 7. Schematic representation of NO_3-anion arrangement between the hydroxide layers.

The average flake size of LDH can be estimated using Scherrer equation [46]:

$$L = K\lambda/\beta cos\theta \quad (1)$$

where L = crystallite size, θ – Bragg angle, β – FWHM (Full Width at Half Maximum) in rad. and K – Scherrer parameter, by default is taken ~0.9. For (hk0) peaks, K is taken to be equal to 1.84 [47].

Reflections (0 0 6) and (1 1 0) were used for the calculation of the average dimensions of the crystallites along *c*-axis and in the direction of *a-b* plane respectively. In this way, an average flake dimension along the a-axis and c-axis of $L_a = 107.0 \pm 7.5$ nm and $L_c = 49.4 \pm 3.4$ nm was obtained Zn-LDH-NO_3, respectively. In the course of the intercalation process with Cl^-, the average flake size becomes smaller in both directions, reaching $L_a = 78.4 \pm 5.5$ nm and $L_c = 30.9 \pm 2.2$ nm.

The X-Ray pattern for Al-LDH-NO_3 has other features. It can clearly be seen, that the LDH reflections, including basal (0 0 3) and (0 0 6)

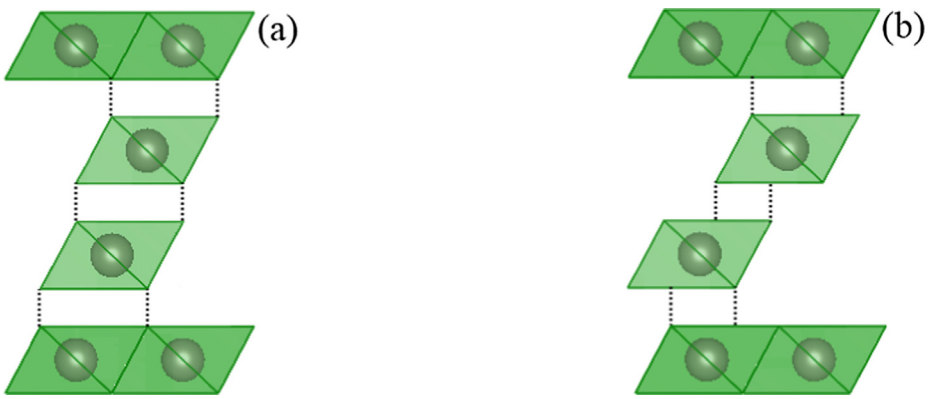

Fig. 6. Schematic representation of 3R1 polytype (a) and $3R_2$ polytype (b).

ones, are asymmetrically broadened (Fig. 5.b). The small sizes of the Al-LDH-NO_3 flakes provide this effect, presumably in combination with the two following factors; i) The first one can be associated with the fact that the planar anions NO_3^- have a coordination symmetry which is different from the one of the interlayer site, hence introducing a significant stacking disorder (turbostratic type in our case) [48]. This could result in a broadening of the non-basal peaks. ii) The second one can be connected with a considerable disorder in the geometrical alignment of NO_3^- anions in between the positively charged layers, which leads to interstratification. This in turn would lead to the broadening and asymmetry of the basal reflections. The absence of the same broadening on X-ray patterns of LDH grown on Zn substrate can mean that LDH growth is highly influenced by nature of the substrate, in other words the source of the generated Al^{3+} and Zn^{2+} cations.

Chloride intercalated Al-LDH-Cl reveals a more ordered structure since the Cl^- anion has a symmetry compatible with that of the interlayer site. However, the non-uniform distribution of the metal cation layers remains still could present, along with small flake size leading to the broadening of (0 0 3) and (0 0 6) reflections for Al-LDH-Cl (Fig. 5.b). Indeed, in the case of Al-LDH-NO_3, the estimation according expression (1) gives some contradictory values like $L_c = 6.9 \pm 0.5$ nm before intercalation and $L_c = 11.5 \pm 0.8$ nm – after the reaction. Thus the broadening of the peaks cannot be attributed entirely to the size effect, and the average size of the flakes cannot be estimated with proper accuracy. Looking into the SEM images for the Al-LDH-NO_3 and Al-LDH-Cl, it can be seen that it is the impractical to draw a conclusion on the basis of the X-ray diffraction pattern solely. The overall morphology and mechanism of LDH growth on AA2024 is governed by a number of factors that can be associated to the complexity of the AA2024 alloy composition [16].

That being said, the shift of the (0 0 3) and (0 0 6) basal reflections into higher angles, after anion-exchange with Cl^- is still a direct consequence of a decrease in the basal spacing. Indeed, the replacement of nitrates (bigger in size) in the LDH interlayers with chlorides (smaller in size) leads to a contraction of the interlayers that manifests by a decrease in the basal spacing [44,45].

The time evolution of the diffraction patterns during anion-exchange process is presented in Fig. 8.

The emergent appearance of the new reflections near the basal ones – (0 0 3) and (0 0 6) – indicates the formation of a new crystal phase and coexistence of two crystal phases during an appreciable time. Thereafter, the basal reflections (0 0 3) and (0 0 6) corresponding to parent crystal phase, eventually disappear.

The fast formation of Zn-LDH-Cl phase in the case of the current experiment, can be detected by the broadening of the basal reflection (0 0 3) at the ~44th second. This broadening is related to the coexistence of both Zn-LDH-NO_3 and Zn-LDH-Cl crystal phases.

The FWHM of the new reflection is comparatively broad and equal to 0.180(10)°, while the peak width of (0 0 3) reflection for the parent Zn-LDH-NO_3 is equal 0.061(2)°. This reflects also the fact that after induction stage, anion-exchange reaction starts from comparatively modest volume, which provides small coherent scattering region (SCSR). The new reflection, corresponding to Zn-LDH-Cl phase becomes narrower when Cl^- replaces NO_3^- and finally the SCSR size effect disappears, leading to FWHM ≈ 0.073(2)°.

For Al-LDH-NO_3, the broadening of the 003 reflection at the ~37th second can be observed indicating the start of the anion exchange process (see Fig. 8.b, arrow). Then as Cl^- replaces NO_3^-, the 003 reflection becomes narrower and more symmetrical in shape.

It can be noted, that the anion exchange process on Zn substrate is faster than on Al substrate. On the latter case, the first exchange occurs rather fast during the first 60 s and continues at a much smoother pace for a duration of approx. 200 s. Whereas, for Zn substrate, the kinetics are different since the overall exchange ceases after about ~70 s.

In addition to the above processes, a strong amorphous phase appears in a considerable amount during the intercalation step for both Zn and Al substrates (Fig. 8). This amorphous phase can be mainly ascribed to the scattering from water. Considering the stability of the crystal structure on both Zn-LDH-NO_3 and Al-LDH-NO_3 with respect to intercalation, it is important to mention that this process is accompanied by a particular decomposition of crystal phase. The decrease of the integrated intensities of the Bragg reflections of the host compounds witnesses about the decrease of the number of the scattering centers. Thus, some remains of the crystalline substance also contribute to the amorphous halo. The time evolution of the volume fraction of the amorphous phase is also demonstrated in Fig. 8. The separation of integral intensities of the crystalline component from the amorphous at the measured diffraction patterns was made using AMORPH software [37].

The structure profile refinement of the chloride-intercalated compounds – Zn-LDH-Cl and Al-LDH-Cl – was made using FAULTS software within rhombohedral R-3m space group and polytypes $3R_1$ and $3R_2$. Examples of refinement are shown in Fig. 9.

The analysis allows to give the preference to $3R_1$ polytype for

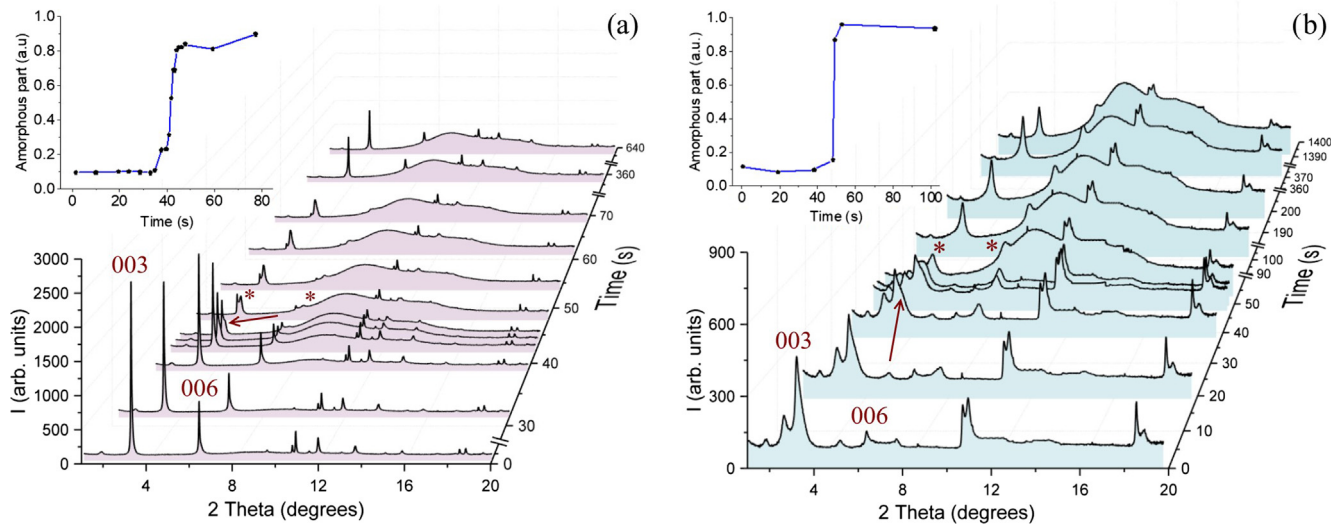

Fig. 8. Timing of X-ray diffraction patterns for LDH-Cl during intercalation process: (a) on Zn substrate; (b) on Al substrate. The contribution from Al peaks was removed for clearance. Indexes 0 0 l indicate the basal peaks of LDH-NO_3, while asterisk (*) indicates the basal peaks of a new LDH-Cl phase. Insets show the change of amorphous phase fraction during the time of anion exchange reaction.

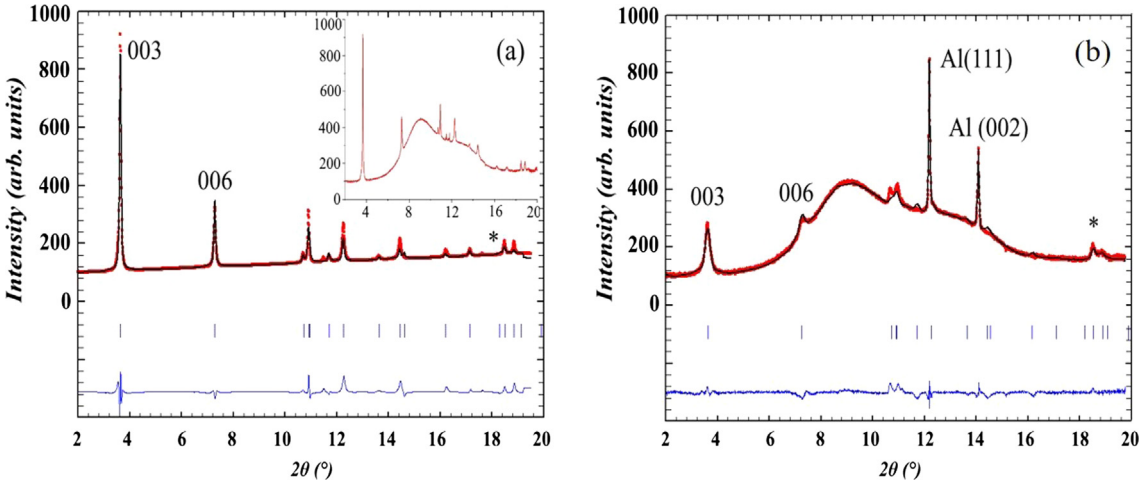

Fig. 9. XRD patterns after anion-exchange reaction of (a) Zn-LDH-Cl with subtracted amorphous contribution (inset shows the full XRD pattern with the amorphous component) and (b) Al-LDH-Cl. Red curves are the observed data, black curves are the calculated patterns, blue lines are the difference profile. Peaks 110/113 are labeled by *.

Table 4
Refined atomic positions of chloride intercalated LDH.

Zn-LDH-Cl						
Layer 1						
Atom	Position	x	y	z	R_p	χ^2
Zn	3a	0	0	0	2.2	0.5
Al	3a	0	0	0		
O_{OH}	6c	0	0	0.374(2)		
O_w	18 h	0.245(32)	0.495(63)	0.5		
Cl	18 h	0.245(32)	0.495(63)	0.5		
Layer 2						
Zn	3a	0	0	0	2.2	0.5
Al	3a	0	0	0		
O_{OH}	6c	0	0	0.374(2)		
O_w	18 h	0.881(5)	−0.881(5)	0.5		
Cl	18 h	0.881(5)	−0.881(5)	0.5		
Al-LDH-Cl						
Atom	Position	x	y	z	R_p	χ^2
Zn	3a	0	0	0	1.9	0.5
Al	3a	0	0	0		
O_{OH}	6c	0	0	0.377(8)		
O_w	18 h	0.860(7)	−0.860(7)	0.5		
Cl	18 h	0.860(7)	−0.860(7)	0.5		

LDH–Cl on Zn substrate (see Fig. 6.a). For Zn-LDH-Cl, the best fit was obtained using model with two different gallery types with both O_w and Cl^- located at 18 h site, but with different coordinates (see Table 4). The cations are located on the 3*a* site, hydroxyl groups are distributed on the 6*c* site. The analysis did not allow the deduction of any kind of preferential stacking for Al-LDH-Cl. This can be the result of a turbostratic disorder of the cation layers as it was previously mentioned, which are preserved in the intercalated substance. The best fit for chloride intercalated Al-LDH-Cl gives a model where atoms Cl occupy the positions corresponding to gallery type 2 in Zn-LDH-Cl. A graphic representation of the galleries' structure is illustrated in Fig. 10.

The unit cell parameters for Zn-LDH-Cl and Al-LDH-Cl are specified in Table 3. These unit cell parameters are compared to respective parental LDH–NO_3 accordingly. As expected, there is no influence on the structure of the metal hydroxide layers arising due to the intercalation process, while the difference between values of *c*-parameters indicates a decrease of the interlayer distance. The gallery heights *h*, for both LDH layers were estimated by subtracting the value of hydroxide layer thickness from basal spacing *d*, which can be calculated as *c*/3. The value of the layer thickness for Zn-based LDH was taken from a previous work [49] and is equal to 0.471 nm. The obtained values (*h*) are also presented in Table 3.

Overall, there is a coherent relation between the morphology of the LDH film observed with SEM images, their elemental analysis obtained by EDS mapping and the crystal structure refinements deduced from the X-ray diffraction data obtained by the *in-situ* synchrotron diffraction measurements. The driving mechanism for LDH growth on the zinc and AA2024 substrate is clearly distinct. This can be already seen from the thickness of the LDH layers (ca. 12 µm for LDH on zinc to ca. 1 µm to LDH on AA2024, Fig. 2).

A relevant observation to add for the case of the AA2024 substrate, is that the presence of intermetallics led to an inhomogeneous size distribution that manifested by zones with large LDH islands (Fig. 3.e – f), as already stated above and in previous studies [38,40].

The LDH growth on Al involves a dissolution of the aluminum oxide layer liberating the desired aluminate ions that then react with zinc

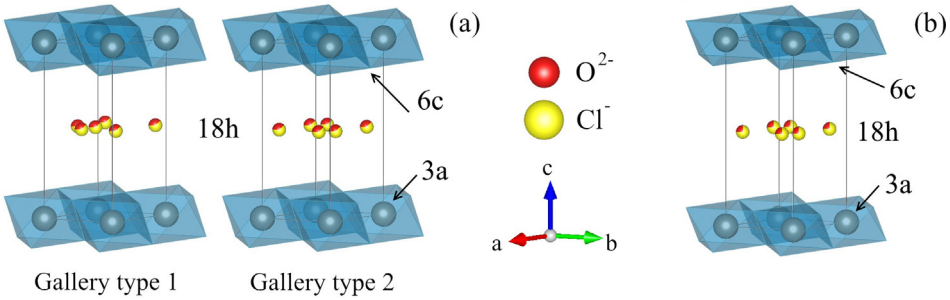

Fig. 10. The arrangement of atoms in the 1st and in the 2nd gallery types obtained from the refinement process of a) Zn-LDH-Cl and b) Al-LDH-Cl. Two colors of one atom mean that either Cl^- or water oxygen O^{2-} takes this position with difference in occupancies (the ratio between these two atoms are shown below).

cations and other relevant species to form Zn-Al LDH [20]. Around the intermetallic zones (especially Cu-rich intermetallic zones that possesses a much more positive potential in comparison to the Al matrix and cause micro-galvanic coupling [50,51]), a different dissolution process is governing. The latter are much more complex and could have affected the course of the LDH growth in terms of kinetics and final LDH composition around this area. This results in significantly higher challenges to obtain concrete information regarding the crystallite size calculations of the Al-LDH-NO_3 and Al-LDH-Cl following the anion-exchange reaction with chlorides.

In terms of kinetics of the anion-exchange reaction, additional studies are also required. A change in the crystalline size of the LDH on Zn substrate in comparison with LDH on AA2024 aluminum alloy was determined based on the XRD results evaluation. However, this change cannot be observed from SEM images. Moreover, other factors related to the rearrangement of the interlayer anion (NO_3^-) during the exchange reaction could not be clearly explained for now.

Regardless, a hypothesis can be emitted, that while charging the cationic Zn:Al host layer is close to 2:1 [45], the NO_3^- are oriented almost vertically, this leads to the gallery height to expand making it easier for the Cl^- anions to enter the galleries. The fast exchange rate between NO_3^- and Cl^- confirms this statement. On the other hand, at lower charge of the cationic host layers (higher Zn to Al ratio), the NO_3^- anions will be positioned in a parallel manner to cation layer [43]. Therefore, Cl^- anions will not be able to enter into galleries so quickly, thus reducing the exchange reaction rate. However, this remains a hypothesis and needs a profound study and investigation and will be taken into consideration in the future.

4. Conclusions

A thorough crystal structure study has been performed in order to compare LDH grown directly on two different substrates (AA2024 and pure zinc). For this purpose, SEM/EDS examination and X-ray diffraction measurements were used. The combination of these methods allowed the establishment of the following points:

- The overall parent LDH-NO_3 structure is similar for both cases. LDH grown on Zinc and AA2024, both belong to the hexagonal lattice group with rhombohedral space group R-3m. The main difference resides in the flake size of LDH grown on Zn and AA2024 substrates.
- After anionic exchange with Cl^-, no changes on the metal hydroxide layers on the different substrates have been depicted from the SEM images. However, the calculation for Zn-LDH-Cl revealed a decrease of the LDH crystallite size. Moreover, the crystal structure refinement reported a different interlayer arrangement for Zn-LDH-Cl, while the Al-LDH-Cl exhibits the same interlayers.

In this work, the importance of the kinetics aspect of the anion exchange reaction and the influence of the interlayer anion rearrangement on the process was perceived. Aside from performing a more precise study about the influence of the substrate composition on LDH growth, it would be also necessary to carry out a systematic study of anion-exchange reactions with various anions to establish a clear pattern and obtained more valuable mechanistic information.

Declaration of Competing Interest

There are no conflicts to declare.

Acknowledgements

We acknowledge DESY (Hamburg, Germany), a member of the Helmholtz Association HGF, for the provision of experimental facilities. Parts of this research were carried out at PETRA III under the proposal number I-20170366. We would like to thank Dr. Sergey Volkov for assistance in using the diffractometer in P08 high-resolution diffraction beamline.

A.C.B and M.H.I are grateful for the financial support of the German-Russian Interdisciplinary Science Center (G-RISC) in form of a travel grant (T-2018b-1 and T-2018a-3 respectively) that enables them to perform a scientific exchange and complete this work.

K.Y. thanks financial support of a researcher grant (IF/01284/2015) and the project CICECO-Aveiro Institute of Materials, FCT Ref. UID/CTM/50011/2019, financed by national funds through the FCT/MCTES, and when appropriate co-financed by FEDER under the PT2020 Partnership Agreement.

M.S. and M.L.Z. are thankful to I2B fond for financial support of this work in frame of MUFfin project as well as the ACTICOAT project (Era.Net RUS Plus Call 2017, Project 477). This research was also partially supported by the European project MULTISURF “MULTI-functional metallic SURFaces via active Layered Double Hydroxide treatments” (REA-Horizon2020-RISE-645676).

References

[1] K. Ogle, R.G. Buchheit, Conversion Coatings: In Encyclopedia of Electrochemistry 4 Wiley-VCH Verlag GmbH & Co. KGaA, 2007, pp. 460–499.
[2] R.G. Buchheit, A.E. Hughes, Chromate and chromate-free conversion coatings, ASM Handbook vol. 13A, (2003).
[3] T. Sankara Narayanan, Surface pretreatment by phosphate conversion coatings-A review, Rev. Adv. Mater. Sci. 9 (2005) 130–177.
[4] A. Reghuraj, K. Saju, Black oxide conversion coating on metals: A review of coating techniques and adaptation for SAE 420A surgical grade stainless steel, Mater. Today:. Proc. 4 (2017) 9534–9541.
[5] A. De Nicolò, L. Paussa, A. Gobessi, A. Lanzutti, C. Cepek, F. Andreatta, L. Fedrizzi, Cerium conversion coating and sol–gel multilayer system for corrosion protection of AA6060, Surf. Coat. Technol. 287 (2016) 33–43.
[6] B. Ramezanzadeh, H. Vakili, R. Amini, Improved performance of cerium conversion coatings on steel with zinc phosphate post-treatment, J. Ind. Eng. Chem. 30 (2015) 225–233.
[7] S. Pommiers, J. Frayret, A. Castetbon, M. Potin-Gautier, Alternative conversion coatings to chromate for the protection of magnesium alloys, Corros. Sci. 84 (2014) 135–146.
[8] W.G. Fahrenholtz, M.J. O'Keefe, H. Zhou, J. Grant, Characterization of cerium-based conversion coatings for corrosion protection of aluminum alloys, Surf. Coat. Technol. 155 (2002) 208–213.
[9] Z. Gao, D. Zhang, X. Li, S. Jiang, Q. Zhang, Current, status, opportunities and challenges in chemical conversion coatings for zinc, Colloid. Surf. A Physicochem. Eng. Asp. 546 (2018) 221–236.
[10] M.F. Montemor, Functional and smart coatings for corrosion protection: a review of recent advances, Surf. Coat. Technol. 258 (2014) 17–37.
[11] I.S. Cole, Handbook of smart coatings for materials protection, Elsevier, Woodhead Publishing Limited, Cambridge United Kingdom, 2014, pp. 29–55.
[12] F. Maia, J. Tedim, A.D. Lisenkov, A.N. Salak, M.L. Zheludkevich, M.G.S. Ferreira, Silica nanocontainers for active corrosion protection, Nanoscale 4 (2012) 1287–1298.
[13] D. Grigoriev, Intelligent coatings for corrosion control, Elsevier, 2015, pp. 283–333.
[14] M. Montemor, Smart composite coatings and membranes, Elsevier, 2016, pp. 183–209.
[15] Q. Wang, D. O'Hare, Recent advances in the synthesis and application of layered double hydroxide (LDH) nanosheets, Chem. Rev. 112 (2012) 4124–4155.
[16] J. Tedim, M.L. Zheludkevich, A.N. Salak, A.D. Lisenkov, M.G.S. Ferreira, Nanostructured LDH-container layer with active protection functionality, J. Mater. Chem. 21 (2011) 15464–15470.
[17] K. Hoshino, S. Furuya, R.G. Buchheit, Effect of NO3− intercalation on corrosion resistance of conversion coated Zn-Al-CO3 LDHs on electrogalvanized steel, J. Electrochem. Soc. 165 (2018) C461–C468.
[18] F. Wang, Z. Guo, Insitu growth of durable superhydrophobic Mg–Al layered double hydroxides nanoplatelets on aluminum alloys for corrosion resistance, J. Alloy. Comp. 767 (2018) 382–391.
[19] M. Zhou, X. Pang, L. Wie, K. Gao, Insitu grown superhydrophobic Zn–Al layered double hydroxides films on magnesium alloy to improve corrosion properties, Appl. Surf. Sci. 337 (2015) 172–177.
[20] M. Serdechnova, M. Mohedano, B. Kuznetsov, C. Mendis, M. Starykevich, S. Karpushenkov, J. Tedim, M. Ferreira, C. Blawert, M. Zheludkevich, PEO coatings with active protection based on in-situ formed LDH-nanocontainers, J. Electrochem. Soc. 164 (2017) C36–C45.
[21] A.I. Khan, D. O'Hare, Intercalation chemistry of layered double hydroxides: recent developments and applications, J. Mater. Chem. 12 (2002) 3191–3198.
[22] X. Duan, D.G. Evans, Layered double hydroxides, Springer Science & Business Media, 2006.
[23] X. Duan, J. Lu, D.G. Evans, Modern inorganic synthetic chemistry, Elsevier (2011) 375–404.
[24] P. Nalawade, B. Aware, V. Kadam, R. Hirlekar, Layered double hydroxides: A review, J. Sci. Ind. Res. 68 (2009) 267–272.

[25] M. Zheludkevich, S. Poznyak, L. Rodrigues, D. Raps, T. Hack, L. Dick, T. Nunes, M.G.S. Ferreira, M. Zheludkevich, S. Poznyak, L. Rodrigues, D. Raps, T. Hack, L. Dick, T. Nunes, M.G.S. Ferreira, Corr. Sci. 52 (2010) 602–611.
[26] J. Tedim, A. Kuznetsova, A.N. Salak, M.F. Montemor, D. Snihirova, M. Pilz, M.L. Zheludkevich, M.G.S. Ferreira, Polyelectrolyte-modified layered double hydroxide nanocontainers as vehicles for combined inhibitors, Corros. Sci. 55 (2012) 1–4.
[27] S.K. Poznyak, J. Tedim, L.M. Rodrigues, A.N. Salak, M.L. Zheludkevich, L.F.P. Dick, M.G.S. Ferreira, Novel inorganic host layered double hydroxides intercalated with guest organic inhibitors for anticorrosion applications, ACS Appl. Mater. Interfaces 1 (2009) 2353–2362.
[28] M. Iqbal, M. Fedel, Effect of synthesis conditions on the controlled growth of MgAl–LDH corrosion resistance film: structure and corrosion resistance properties, Coatings 9 (2019) 30.
[29] Y. Zhang, J. Liu, Y. Li, M. Yu, S. Li, B. Xue, Fabrication of inhibitor anion-intercalated layered double hydroxide host films on aluminum alloy 2024 and their anticorrosion properties, J. Coat. Technol. Res. 12 (2015) 293–302.
[30] R.G. Buchheit, S.B. Mamidipally, P. Schmutz, H. Guan, Active corrosion protection in Ce-modified hydrotalcite conversion coatings, Corrosion. 58 (2002) 3–14.
[31] R.G. Buchheit, H. Cuan, Formation and characteristics of Al− Zn hydrotalcite coatings on galvanized steel, J. Coat. Technol. Res. 1 (2004) 277–290.
[32] T. Ishizaki, S. Chiba, K. Watanabe, H. Suzuki, Corrosion resistance of Mg–Al layered double hydroxide container-containing magnesium hydroxide films formed directly on magnesium alloy by chemical-free steam coating, J. Mater. Chem. A 1 (2013) 8968–8977.
[33] G. Zhang, L. Wu, A. Tang, X.B. Chen, Y. Ma, Y. Long, P. Peng, X. Ding, H. Pan, F. Pan, Growth behavior of MgAl-layered double hydroxide films by conversion of anodic films on magnesium alloy AZ31 and their corrosion protection, Appl. Surf. Sci. 456 (2018) 419–429.
[34] A. Mikhailau, H.M. Maltanava, S.K. Poznyak, A.N. Salak, M.L. Zheludkevich, K.A. Yasakau, M.G.S. Ferreira, One-step synthesis and growth mechanism of nitrate intercalated ZnAl LDH conversion coatings on zinc, ChemComm. 55 (2019) 6878–6881.
[35] O.H. Seeck, C. Deiter, K. Pflaum, F. Bertam, A. Beerlink, H. Franz, J. Horbach, H. Schulte-Schrepping, B.M. Murphy, M. Greve, O. Magnussen, The high-resolution diffraction beamline P08 at PETRA III, J. Synchrotron. Rad. 19 (2012) 30–38.
[36] Montse Casas-Cabanas, Marine Reynaud, Jokin Rikarte, Pavel Horbach, Juan Rodríguez-Carvajal, FAULTS: a program for refinement of structures with extended defects, J. Appl. Crystallogr. 49 (6) (2016) 2259–2269, https://doi.org/10.1107/S1600576716014473 10.1107/S1600576716014473/kc5049sup1.pdf 10.1107/S1600576716014473/kc5049sup2.txt 10.1107/S1600576716014473/kc5049sup3.txt 10.1107/S1600576716014473/kc5049sup4.txt.
[37] M.C. Rowe, B.J. Brewer, AMORPH: A statistical program for characterizing amorphous materials by X-ray diffraction, Comput. Geosci. 120 (2018) 21–31.
[38] T.H. Muster, A.E. Hughes, G.E. Thompson, Copper distributions in Al-alloys, Vic and Clayton, CSIRO Materials Science and Engineering, Corrosion Research Trends, Nova Publishing, England, 2007, pp. 35–106.
[39] M. Mokaddem, P. Volovitch, F. Rechou, R. Oltra, K. Ogle, The anodic and cathodic dissolution of Al and Al–Cu–Mg alloy, Electrochim. Acta 55 (2010) 3779–3786.
[40] M. Serdechnova, P. Volovitch, F. Brisset, K. Ogle, On the cathodic dissolution of Al and Al alloys, Electrochim. Acta 124 (2014) 9–16.
[41] M.L. Zheludkevich, A.C. Bastos, A.N. Salak, J. Carneiro, F. Maia, A.D. Lisenkov, A.B. Oliveira, M.G.S. Ferreira, Effect of surface treatment on the performance of LDH conversion films, ECS Electrochem. Lett. 3 (2014) C4–C8.
[42] W. Zhang, K. Yanagisawa, Hydrothermal synthesis of zinc hydroxide chloride sheets and their conversion to ZnO, Chem. Mater. 19 (2007) 2329–2334.
[43] S. Marappa, S. Radha, P.V. Kamath, Nitrate-intercalated layered double hydroxides-structure model, order, and disorder, Eur. J. Inorg. Chem. 2013 (2013) 2122–2128.
[44] M. Serdechnova, A.N. Salak, F.S. Barbosa, D.E. Vieira, J. Tedim, M.L. Zheludkevich, M.G.S. Ferreira, Interlayer intercalation and arrangement of 2-mercapto-benzothiazolate and 1, 2, 3-benzotriazolate anions in layered double hydroxides: in situ X-ray diffraction study, J. Solid State Chem. 233 (2016) 158–165.
[45] D.G. Evans, R.C. Slade, Layered double hydroxides, Springer, 2006, pp. 1–87.
[46] P. Scherrer, Determination of the size and internal structure of colloidal particles using X-rays, Nachr. Ges. Wiss. 2 (1918) 98–100.
[47] B.E. Warren, X-ray diffraction in random layer lattices, Phy. Rev. 59 (1941) 693.
[48] A.V. Radha, P.V. Kamath, C. Shivakumara, Conservation of order, disorder, and “crystallinity” during anion-exchange reactions among layered double hydroxides (LDHs) of Zn with Al, J. Phys. Chem. B 111 (2007) 3411–3418.
[49] M. Serdechnova, V.L. Ivanov, M.R.M. Domingues, D.V. Evtuguin, M.G.S. Ferreira, M.L. Zheludkevich, Photodegradation of 2-mercaptobenzothiazole and 1, 2, 3-benzotriazole corrosion inhibitors in aqueous solutions and organic solvents, PCCP 16 (2014) 25152–25160.
[50] Y. Zhu, K. Sun, G. Frankel, Intermetallic phases in aluminum alloys and their roles in localized corrosion, J. Electrochem. Soc. 165 (2018) C807–C820.
[51] N. Birbilis, R. Buchheit, Electrochemical characteristics of intermetallic phases in aluminum alloys an experimental survey and discussion, J. Electrochem. Soc. 152 (2005) B140–B151.